PCCP

Nitrogen Electroreduction and Hydrogen Evolution on Cubic Molybdenum Carbide: A Density Functional Study

Journal:	*Physical Chemistry Chemical Physics*
Manuscript ID	CP-ART-03-2018-001643.R2
Article Type:	Paper
Date Submitted by the Author:	23-Apr-2018

Complete List of Authors:	Matanovic, Ivana; University of New Mexico, Chemical and Biological Engineering; Los Alamos National Laboratory Garzon, Fernando; University of New Mexico

Journal Name

ARTICLE

Nitrogen Electroreduction and Hydrogen Evolution on Cubic Molybdenum Carbide: A Density Functional Study

Ivana Matanovic[a,b] and Fernando H. Garzon[*a,c]

Received 00th January 20xx,
Accepted 00th January 20xx

DOI: 10.1039/x0xx00000x

www.rsc.org/

We report herein a density functional theory study of the nitrogen electroreduction and hydrogen evolution reaction on cubic molybdenum carbide (MoC) in order to investigate the viability of using this material as an electro-catalyst for ammonia synthesis. Free energy diagrams for associative and dissociative Heyrovsky mechanism showed that the nitrogen reduction on cubic MoC(111) can proceed via an associative mechanism and that small negative potentials of -0.3 V *vs* standard hydrogen electrode can onset the reduction of nitrogen to ammonia. Kinetic volcano plots for hydrogen evolution showed that MoC[110] surface is expected to have a high rate for hydrogen evolution reaction, which could compete with the reduction of nitrogen on cubic MoC. The comparison between the adsorption energies of H-adatoms and N-adatoms also shows that at low potentials adsorption of hydrogen atoms competes with nitrogen adsorption on all the MoC surfaces except the MoC(111) surface. The hydrogen evolution and accumulation of H-adatoms can be mitigated by introducing carbon vacancies i.e. increasing the ratio of metal to carbon atoms, which will significantly increase the affinity of the catalytic surface for both nitrogen molecules and N-adatoms.

1. Introduction

Ammonia is one of the most important industrial chemicals with the world's annual production that exceeds 200 million tons.[1] Current industrial process for ammonia synthesis still relies on a century old Haber-Bosch process, in which ammonia is produced from nitrogen and hydrogen using Fe- or Ru-based catalysts at high operating pressure and temperature. This production process requires a significant energy input, which annually consumes around 1.4% of global energy resources.[2] High-energy demands and extreme conditions required in the Haber-Bosch process have inspired intense research into alternative production routes, such as electrochemical synthesis of ammonia from nitrogen, protons, and electrons at ambient conditions. Since it was first demonstrated almost two decades ago,[3] the electrochemical synthesis of ammonia has been studied in a variety of experimental configurations and conditions.[4] Namely, the electrochemical path offers several techno-economic benefits over Haber-Bosch process including the use of ionic membranes that allows a selective transfer of the protons to the cathode side and prevents poisoning of the catalyst with the impurities in the hydrogen gas. Electrochemical synthesis of ammonia also allows for the potential elimination of gaseous hydrogen from the process as stream and water can be used as alternative sources of hydrogen.

Although electrochemical methods for ammonia synthesis have not yet been realized on the industrial scale, significant advances have been made in the last decade.[4] This can mainly be attributed to the development of new proton conducting membranes and exploration of various materials used as electro-catalysts. These include transition metals, Pt, Pd, Ru, Fe, Ni, Ni-Cu, conductive oxides and various composite materials, such as mixed oxides and perovskites.[4] However, the pursuit of an ideal electro-catalyst that exhibits high catalytic activity and conductivity while at the same time suppresses the competing hydrogen evolution reaction at ambient conditions is still an on-going effort.

Theoretical studies and computational modelling play a key role in predicting promising catalytic materials,[5] including the electro-catalysts for nitrogen reduction.[6-15] The most notable example is the Co-Mo catalyst, which was designed based on the adsorption energy of nitrogen molecule on transition metal surfaces, and was confirmed through later experimental studies of ammonia electro-synthesis on Co_3Mo_3N nitride.[6, 16] Skúlason et al. were the first to present a detailed DFT study for possible transition-metal electro-catalysts and determined Sc, Y, Ti, and Zr, as possible selective electro-catalysts for nitrogen reduction to ammonia.[7] Abghoui et al. further studied thermodynamics of the nitrogen electro-reduction on 26 different d-block metal mononitrides and found that ZrN, NbN, CrN, and VN are expected to be more active toward nitrogen reduction than toward the competing reaction of hydrogen evolution.[13, 14]

In this work, we use density functional theory to explore the possibility of using cubic MoC as an electro-catalyst for reduction of nitrogen to ammonia. Due to their low cost and unique chemical and physical properties, earth abundant transition metal carbides

[a] *Chemical and Biological Engineering Department, Center for Micro-Engineered Materials, University of New Mexico, Albuquerque, NM 87131, USA*
[b] *Theoretical Division, Los Alamos National Laboratory, Los Alamos, NM 87545, USA*
[c] *Sandia National Laboratory, Albuquerque, NM 87131, USA*
* garzon@unm.edu

have proven as promising catalysts for a variety of reactions, such as alcohol electrooxidation[17], water electrolysis[18], biomass conversion[18], water gas shift reaction,[19, 20] and ammonia decomposition.[21] Moreover, it was previously shown that a number of interstitial alloys formed by the incorporation of carbon, nitrogen, and oxygen into the lattices of metals, including molybdenum carbide and nitride, show activity for ammonia synthesis.[22, 23] Our previous computational work has also shown that the molybdenum nitride, isostructural to cubic MoC shows promise as a selective catalyst for ammonia electro-synthesis.[11] Namely, we have found that the Mo_2N(111) surface can reduce nitrogen at negative cell potentials of -0.7 V *vs* standard hydrogen electrode. The production of hydrogen at these potentials is suppressed due to the high affinity of this surface for N-adatoms.

Molybdenum carbide exists in several phases, including hexagonal, cubic, and orthorhombic phase with differing stoichiometries, but the literature reports of the exact phase behaviour are somewhat contradictory.[24, 25] The cubic phase can be obtained by temperature programmed reaction method using mixtures of hydrogen and methane, hydrogen and ethane, and hydrogen and butane as carburizing agents.[26, 27] For instance, metastable cubic MoC_{1-x} (x ~0.5) unsupported powders were prepared by temperature-programmed reaction of MoO_3 with ammonia and CH_4/H_2 mixture.[27] In addition, phase relations between the molybdenum carbides, nitrides, and oxides are extremely complex and not well understood[28-30], which hinders establishing clear correlations between the catalytic activity and the materials' chemical structure. The issue can be partially mitigated by the density functional theory studies of the ammonia electroreduction on well-defined models. The current study includes different surfaces of cubic molybdenum carbide and aims at establishing general trends in the reactivity of the cubic molybdenum carbide toward two competing reactions, nitrogen electroreduction and hydrogen evolution reaction, and also includes comparison to the isostructural molybdenum nitride surfaces. Furthermore, we were also interested to learn how metal to carbon ratio affects the reactivity and selectivity of the MoC cubic phase as it was found that the metal to carbon ratio plays a key role in defining activity, selectivity, and stability of CO_2 reduction to CO[31] and water gas shift reaction[32] on bifunctional Au/δ-MoC and Cu/δ-MoC catalysts. Other stable phase of molybdenum carbide with Mo:C ratio of 2:1, hexagonal Mo_2C, was previously studied as a catalyst for ammonia decomposition[21] and was also proven to be a good catalyst for hydrogen evolution reaction[33-35] and will be excluded from this study.

2. Computational Details

Density Functional Theory (DFT) calculations were performed using generalized gradient approximation approach (GGA) with the Perdew-Burke-Ernzerhof (PBE) functional[36, 37] and projector augmented-wave pseudopotentials[38, 39] as implemented in Vienna ab initio simulation package [40-43]. The MoC in a cubic phase (Fm-3m space group) was modelled using the DFT optimized unit cell of the size a=b=c=4.34 Å and α=β=γ=90°, which in good agreement with the experimental values of a=b=c=4.27 Å and α=β=γ=90° (ICDD card 01-073-9798). In order to study the effect of metal to carbon ratio on the activity and the selectivity of the molybdenum carbide, we created a substoichiometric $MoC_{0.5}$ composition from a cubic MoC structure by removing half of the carbon atoms in the 100/010 direction in order to obtain 2:1 ratio of Mo and C atoms. By introducing the carbon vacancies the structure became tetragonal with the optimized cell parameters determined as 4.23 Å and 4.26 Å, which is in good agreement with the cell parameters of 4.23 – 4.28 Å that were reported for metastable cubic MoC_{1-x} with x=0.25-0.5 [27]. This structure is also isostructural to previously studied fcc γ-Mo_2N.[11] In order to study the reactivity of different surfaces, we considered [100], [110], (111), and (311) surfaces of MoC (Figure 1a). In the case of $MoC_{0.5}$ composition equivalent (001), (100)/(010), (101), and (311) surfaces were considered (Figure 1b). The effect of defects and under-coordinated Mo was studied by using the (111) surfaces in which defects were introduced by removing two Mo atoms from the top layer (denoted as (111)*). The same approach was used to study the influence of Mo defects on the reactivity of molybdenum nitride.[11]

All the surfaces were modelled using the 2x2 super-cells with 4 layers of metal atoms and a vacuum region of 15 Å. During the optimizations two top layers containing Mo atoms together with the adsorbed species were allowed to relax until all forces acting on them were smaller than 0.01 eV $Å^{-1}$ while the two bottom layers were held fixed. The electronic energy convergence was set to $1x10^{-5}$ eV. In all the cases, calculations were done as spin-polarized with dipole correction applied in the direction normal to the surface and with the plane-wave basis cut-off was set to 755 eV. The calculation were performed with 4x4x1 k-point Monkhorts-Pack[44] mesh and Methfessel-Paxton smearing[45] of order 1 with σ =0.05. The adsorption energies (ΔE_{ad}) were calculated using the following formula:

$$\Delta E_{ad} = E_{surface+ad} - \left[E_{surface} + E_{ad}\right]$$

where $E_{surface+ad}$ is the energy of species adsorbed on the surface, $E_{surface}$ is the energy of the clean surface, and E_{ad} is the energy of the corresponding species in the gas phase.

The changes in the Gibbs free energies for the nitrogen electroreduction were calculated as

$$\Delta_r G = \Delta E_{ad} + \Delta ZPE - T\Delta S$$

where ΔZPE is the change in the zero point energy and ΔS is the change in entropy during the reaction. Zero point energies were calculated using the vibrational frequencies obtained from a normal mode analysis of reactants and products in the gas phase and of the intermediates adsorbed on the surface while the change in the entropy was calculated using the gas phase values from the thermodynamic tables.[46] The concept of computational hydrogen electrode was used to relate the chemical potential of the electron/proton pair to that of the $1/2H_2$(g).[47, 48]

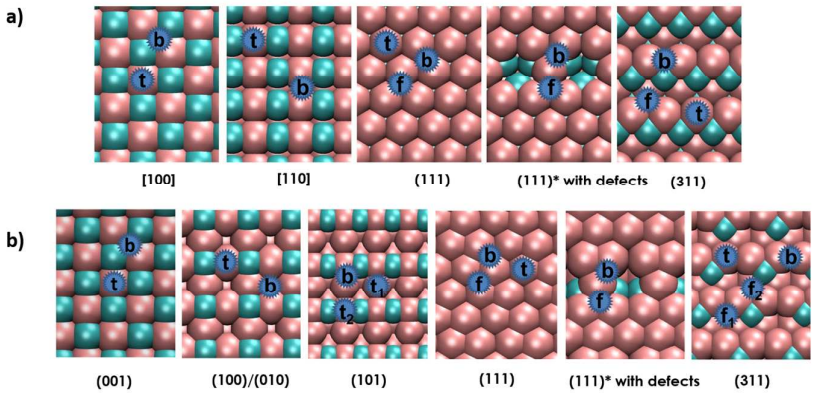

Figure 1. Model surfaces of cubic a) MoC and b) $MoC_{0.5}$ compositions used with different non-equivalent adsorption sites for H and N-adatoms. Asterisk (*) denotes the (111) surface with Mo-defects introduced. Top adsorption sites are denoted with *t*, bridge sites with *b*, and fcc sites are denoted with *f*. Pink – Mo, green – C atom.

3. Results and discussion

3.1. Hydrogen evolution reaction.

Adsorption energies of hydrogen atom were calculated on different surfaces of a cubic MoC and $MoC_{0.5}$ and given in Table 1. The results show that in both cases low index MoC[100] and $MoC_{0.5}$(001) surface have a weak interaction with hydrogen, while (111), (311) and (111) surface with defects for both compositions have high interaction with the hydrogen atoms. Namely, the adsorption energy of the hydrogen atom on MoC[100] and $MoC_{0.5}$(001) surfaces are calculated as -2.07 eV and -2.13 eV, respectively, while the adsorption energies calculated for (111), (111)* and (311) surfaces of MoC and $MoC_{0.5}$ excede -3.03 eV. Larger adsorption energies on (111), (111)* and (311) surface can be attributed to the adsorption of hydrogen atoms to high coordination bridging and fcc sites that enables interaction of H-adatom with two or three surface metal atoms. The adsorption energies of H atom from Table 1 are used to calculate the free energy diagams for hydrogen evolution reaction (HER) and compared to that of Pt(111), which is well know HER catalyst (Figure 2). In this case, the HER mechanism was described by three state diagram corresponding to the proton electron pair ($H^+ + e^-$) , adsorbed H (*H) and a final product hydrogen molecule ($1/2H_2$).[49, 50] The strength of the interaction between the hydrogen atom and the surface defines the Gibbs free energy of the adsorbed hydrogen (ΔG_{*H}), which is an established descriptor of HER activity. The optimum value of ΔG_{*H} for an ideal HER catalysts would be zero indicating the best electrocatalytic performance from the viewpoint of thermodynamics. For instance, this value for the metal catalysts with high HER activity such as Pt, Pd, and Rh is very close to 0 eV. More specifically, ΔG_{*H} for Pt(111) is calculated as -0.09 eV, which is in excellent agreement with previous calculations.[49, 51] Comparing this value with the values calculated for different surfaces of MoC and $MoC_{0.5}$, we can predict that the dissociative adsorption of hydrogen on the MoC[100] surface is too weak with very positive ΔG_{*H} indicating easy product desorption. Dissociative adsorption of hydrogen on (111) and (311) surfaces for both compositions, on the other hand, is too strong with largly negative ΔG_{*H}. High HER activity from the thermodynamic point of view is predicted for MoC[110], followed by $MoC_{0.5}$(100) and $MoC_{0.5}$(101) surface. Namely, the Gibbs free energy for the dissociative adsorption of hydrogen on these surfaces was calculated as -0.12 eV, -0.25 eV, and -0.29 eV, respectively. The result indicates that the MoC[110] surface is expected to have high activity for HER, which will compete with the reduction of nitrogen. Increasing metal to carbon ratio will increase the change in the free energy for hydrogen desorption on this surface and to some extent decrease the activity for HER.

Table 1. Adsorption energies (ΔE_{ad}) in eV of H atom on different MoC and $MoC_{0.5}$ surfaces. The reference state of hydrogen is H atom in the gas phase.

MoC	[100]	[110]	(111)	(111)*	(311)	
ΔE(H) top	-2.07	bridge	-2.90	fcc	-2.78	
ΔE(H) bridging	top	-2.77	fcc	-3.25	-3.03	
ΔE(H) fcc			-3.26	-3.30	bridge	
$MoC_{0.5}$	(001)	(100/010)	(101)	(111)	(111)*	(311)
ΔE(H) top	-2.13	-1.90	bridge	fcc	fcc	bridge
ΔE(H) bridging	top	-2.96	-3.00	fcc	-3.15	-3.50
ΔE(H) fcc				-3.37	-3.31	-2.98

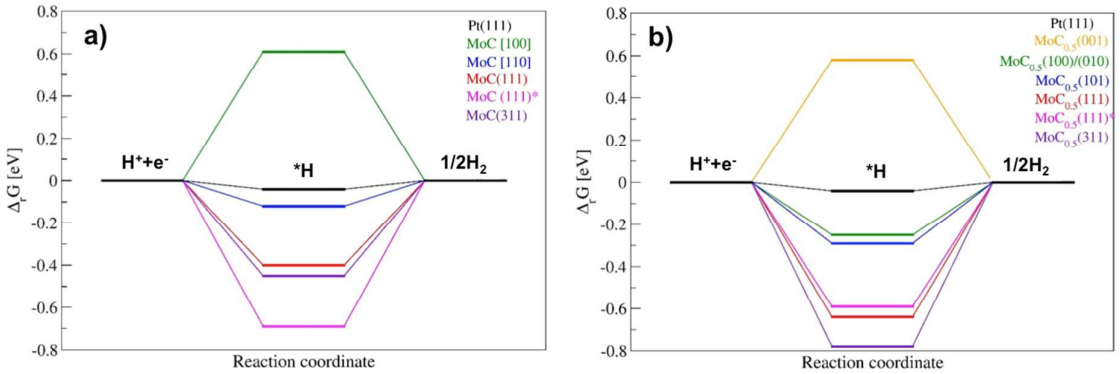

Figure 2. Free energy diagram for hydrogen evolution (U = 0 V) calculated from DFT energies for the intermediate adsorbed state (0.5 ML coverage) for cubic a) $MoC_{0.5}$ and b) MoC. The data are given for standard conditions corresponding to 1 bar of H_2 and pH=0 at 300K.

It was previously established that the kinetics of HER on metallic surfaces follows the volcano curve if the experimentally measured exchange current, log(i_0) is plotted against the free energy of the adsorbed hydrogen, $\Delta G_{*H.}$[49, 51] On this plot (Figure 3) MoC[001] and $MoC_{0.5}$(001) are situated on the far right side of the volcano curve while $MoC_{0.5}$(311), $MoC_{0.5}$(111), and (111)* surfaces of MoC and $MoC_{0.5}$ are situated far left on the volcano plot. Both positions indicate decreased rate of HER. Namely, on the left side of the volcano plot, HER rate decreases as the adsorption energy of hydrogen increases due to the lack of the available sites for H+H recombination while on the right side of the volcano HER is limited by the proton transfer due to low stability of the adsorbed hydrogen.[49]

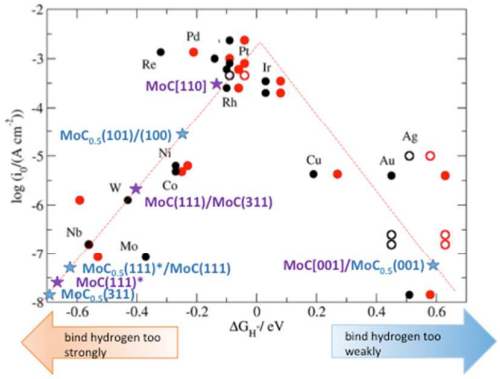

Figure 3. Experimentally measured exchange current, log(i_0) for hydrogen evolution over different metal surfaces plotted as a function of the DFT calculated hydrogen adsorption free energies for 0.25 ML coverage (red) and 1 ML coverage (black). Open circles correspond to single crystal data. Experimental values and DFT values for metal surfaces other than MoC, $MoC_{0.5}$, and Pt taken from Ref[49] and references herein.

MoC[110] surface is the closest to the top of the volcano curve, while MoC(111), MoC(311), $MoC_{0.5}$(100), and $MoC_{0.5}$(101) surfaces are neither too far to the left nor too far to the right of the volcano curve and might show some activity for HER.

Therefore, our results show that cubic MoC is expected to have activity for hydrogen evolution due to the high activity of the MoC[110] surface, which can be decreased by introducing carbon vacancies into the structure. The implications of these results for the nitrogen reduction activity will be discussed in more details in the following sections. Reactivity of the surface at a certain pH and potential depends on the most stable state of the surface (coverage with H or N-adatoms) and will be determined by the relative strength of interaction between the catalytic surface and the H-adatoms or N-adatoms.

3.2. Reactivity towards nitrogen

The adsorption energies of N_2 molecule from Table 2 show that the MoC[100] has the weakest interaction with nitrogen molecule, while the rest of the MoC surfaces have somewhat similar interaction with the nitrogen molecule. Namely, the adsorption energy of N_2 on the MoC[100] surface was calculated as -0.23 eV, while the values in the range from -0.80 eV to -1.06 eV were obtained for the rest of the considered MoC surfaces. The analysis of the results obtained for $MoC_{0.5}$ composition shows that the carbon vacancies in the structure increase the interaction with both nitrogen molecule and N-adatoms. Namely, $MoC_{0.5}$(111) and $MoC_{0.5}$(111)* surface have the strongest interaction with the N_2 molecule, followed by the higher index $MoC_{0.5}$(311) surface. The adsorption energy of nitrogen molecule on $MoC_{0.5}$(111), $MoC_{0.5}$(111)*, and $MoC_{0.5}$(311) surface was calculated as -1.24 eV, -1.65 eV, and -1.60 eV, while it is determined as -1.13 eV, -0.44, and -0.26 eV on the $MoC_{0.5}$(101), $MoC_{0.5}$(100), and $MoC_{0.5}$(001) surface, respectively. Furthermore, it was found that the(111), (111)* and (311) surfaces of both compositions bind N_2 molecule in a perpendicular side-on or a parallel end-on bridging position.

Journal Name

ARTICLE

In these adsorption sites, N_2 molecule is in a bridge between two Mo atoms, but the N-N bond of the N_2 is either perpendicular or parallel to the line connecting the two Mo atoms. Our previous work on molybdenum nitride showed that the bridging coordination of N_2 allows for a larger coupling of metal *d*-states and nitrogen orbitals and, thus, a larger transfer of electron density from the catalytic surface to the antibonding π* orbitals of adsorbed nitrogen.[11] This leads to the activation of the N-N triple bond in the adsorbed N_2 molecule and increases its reactivity. It is interesting to note that in the case of MoC(111)* surface we were not able to stabilize the N_2 adsorbed in side-on position as the molecule would dissociate during the optimization calculation leading to two adsorbed nitrogen atoms. These conclusions are further supported by the structural features of the adsorbed nitrogen molecule on these surfaces, in particular the elongation of the N–N bond after adsorption. For example, the N–N distance of N_2 adsorbed in the perpendicular side-on bridging position on MoC(111) surface is determined to be 1.24 Å as compared to 1.10 Å calculated for N_2 in the gas phase.

The strength of interaction between the N_2 molecule and different surfaces/compositions is reflected in the change of the Gibbs free energy during the N_2 adsorption processes (Figure 4). For nitrogen adsorption to be exergonic, the change in the internal energy has to compensate for the loss of the entropy during the adsorption process. The free energy diagrams for N_2 adsorption show that the adsorption of N_2 is exergonic on all the considered surfaces except the MoC[100], $MoC_{0.5}$(001), and $MoC_{0.5}$(100) surface due to their weak interaction with nitrogen molecule (Figure 2). From the thermodynamic point of view, the spontaneity of the next step i.e. dissociation of the N-N bond in the adsorbed N_2 molecule is determined by the strength of the interaction between the specific surface and the N-adatom. The results, thus, show that the dissociation of N_2 is exergonic on the MoC(111), MoC(111)*, MoC(311) and MoC[100] surfaces.

Table 2. Adsorption energies (in eV) of N_2 molecule and N atom on different cubic MoC and $MoC_{0.5}$ surfaces.

MoC	[100]	[110]	(111)	(111)*	(311)	
Δ*E*(N_2) top	-0.23	-0.80	-0.89	-0.89	-0.77	
Δ*E*(N_2) side-on	-0.05	-0.89	-1.06	dissociates	-0.80	
Δ*E*(N) top	-4.39	-4.39	-4.88	-4.95	-4.88	
Δ*E*(N) bridge	-6.25	-5.48	fcc	fcc	fcc	
Δ*E*(N) fcc	N/A	N/A	-6.86	-6.54	-6.03	
$MoC_{0.5}$	(001)	(100)/(010)	(101)	(111)	(111)*	(311)
Δ*E*(N_2) top	-0.26	-0.44	-0.73	-0.93	-0.74	-0.91
Δ*E*(N_2) side-on	-0.01	-0.01	-1.13	-1.24	-1.65	-1.60
Δ*E*(N) top	-4.33	-3.95	bridge	fcc	fcc	
Δ*E*(N) bridge	top	-5.72	-6.04	fcc	fcc	-7.53
Δ*E*(N) fcc	N/A	N/A	N/A	-7.73	-7.62	-7.28

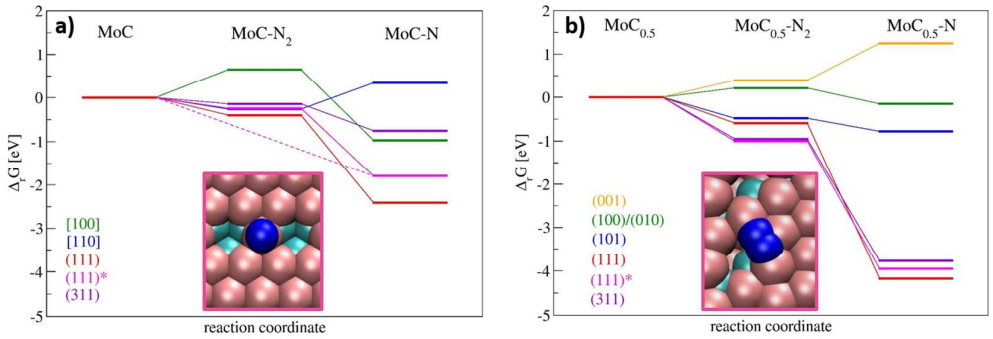

Figure 4. DFT calculated free energy diagram for N_2 adsorption and dissociation on different surfaces of cubic MoC with a) MoC and b) $MoC_{0.5}$ compositions. Nitrogen molecule adsorbed on top end on site on the MoC(111)* surface and parallel end-on bridging site on the $MoC_{0.5}$(111)* surface. Pink – Mo, green –C, blue – N atoms.

Journal Name

ARTICLE

Namely, the change in the Gibbs free energy for the N_2 adsorption and consecutive dissociation of adsorbed N_2 are calculated as -0.40 eV and -2.01 eV on the MoC(111) surface, -0.24 eV and -1.55 eV on the MoC(111)* surface and -0.14 eV and -0.61 eV on the MoC(311) surface, respectively. Therefore, among all the studied surfaces the MoC(111), MoC(111)*, and MoC(311) surface are expected to have the highest activity for N_2 adsorption and dissociation. The activity of MoC(100) and MoC(110) surfaces is expected to be low as MoC(100) has a low affinity for N_2, while on the MoC(110) surface the activity is limited by the N_2 dissociation step. In the case of the $MoC_{0.5}$ composition, (111), (111)* and (311) have the highest interaction with the N-adatom calculated as -7.73 eV, -7.62 eV and -7.28 eV, resulting in a large thermodynamic drive for N_2 dissociation of -3.58 eV, -2.95 eV and -2.83 eV. Therefore, increasing the Mo to C ratio for the (111), (111)*, and (311) surfaces increases their affinity for both nitrogen molecule and N-adatoms (Figure 4).

The Gibbs free energies for dissociation and adsorption of nitrogen atom can be further compared with the free energies for the adsorption of hydrogen atom. Namely the comparison between these two energies i.e. free energies for the $*+1/2N_2 \rightarrow *N$ and $*+H^++e^- \rightarrow *H$ process will determine conditions under which the catalytic surface will be covered with N-adatoms instead of H-adatoms (Figure S1a). On MoC surfaces with high activity for nitrogen adsorption and dissociation, namely MoC(111), MoC(111)*, and MoC(311), the free energy for the formation of N-adatoms is calculated as -1.21 eV, -0.90 eV and -0.38 eV, while the free energy for the formation of H-adatoms is calculated as -0.40 eV, -0.69 eV and -0.45 eV (Table S1). Therefore, hydrogen atoms are expected to accumulate at potentials as low as 0.07 V (the case of the MoC(311) surface). The surface most resistant to the accumulation of H-adatoms is MoC(111) surface on which the adsorption of nitrogen should be thermodynamically more favorable up to the potentials of -0.80 V. In addition, introducing carbon vacancies proves to be beneficial as it will increase the affinity of these surfaces for N-adatoms and prevent accumulation of H-adatoms for up to -1.44 V relative to the standard hydrogen electrode (Figure S1b).

In conclusion, (111), (111)* and (311) surfaces of cubic MoC are predicted to have high activity for N_2 adsorption and activation. Moreover, we have found that the MoC(111)* surface is the only surface with a low kinetic barrier for N_2 dissociation when N_2 molecule adsorbs in the parallel end-on bridging position. However, due to the weaker interaction with N-adatoms, most of the MoC surfaces will accumulate H-adatoms at potentials necessary to drive nitrogen reduction, which can reduce the efficiency of nitrogen reduction to ammonia. Our results also showed that this issue can be mitigated by introducing carbon vacancies in the surface or subsurface layers of the cubic MoC structure. Namely, smaller number of carbon atoms in the coordination shell of the surface Mo atoms creates under-coordinated metal sites with stronger interaction with N_2 and N-adatoms. The similar effect of under-coordinated surface Mo-atoms was observed with Mo_2N. In addition, previous studies have emphasized the importance of the under-coordinated sites on the surface of the catalyst as these sites often dominate the catalytic activity of the catalyst.[13]

3.3. Electroreduction of nitrogen to ammonia

We further studied the Gibbs free energy change for the elementary steps in the electroreduction of nitrogen to ammonia on two representative surfaces of MoC and $MoC_{0.5}$ compositions, namely the MoC(111) and $MoC_{0.5}$(111) surfaces. The Heyrovsky-type mechanism was considered that can either be of associative or dissociative nature.[52] In the dissociative Heyrovski mechanism adsorbed nitrogen molecules first undergo dissociation on the surface after which adrobed nitrogen atoms are hydrogenated by the protons in the solution (Figure 5a).

In the associative path, nitrogen molecule is first hydrogenated with multiple protons from the solution followed by the N-N bond-breaking step in one of the adsorbed N_2H_y species (Figure 5b). According to the Sabatier principle the optimal catalysts would have neither too strong nor too weak interaction with all the intermediates in the reaction leading to the reaction mechanism with exothermic steps.

3.3.1. Dissociative mechanism

Our DFT results show that on the MoC(111) surface the first four steps in the dissociative mechanism of nitrogen electroreduction to ammonia are exergonic (Figure 5a). The free energy change for the adsorption of nitrogen, dissociation of the adsorbed nitrogen molecule to adsorbed N atoms, and the formation of *NH from *N are calculated as -0.41 eV, -2.0 eV, and -0.47 eV, respectively. The formation of adsorbed $*NH_2$ from adsorbed *NH ($*NH+H^++e^- \rightarrow *NH_2$) requires the largest amount of energy on the MoC(111) surface i.e. +0.44 eV. This indicates that the potential of at least -0.44 V relative to standard hydrogen electrode is needed to drive the reduction of nitrogen to ammonia on MoC. However, the desorption of ammonia from the MoC(111) surface is 0.6 eV uphill and this step becomes the thermodynamically limiting step for the nitrogen reduction at the cell potentials lower than -0.44 V. As this step does not involve electron transfer, it cannot be tuned by applying external potential and can become slower at low temperatures leading to the poisoning of the catalytic surface with the product of the reaction.

Journal Name

ARTICLE

Table 3. DFT calculated adsorption energies (in eV) of different intermediates in N_2 electroreduction on $MoC_{0.5}$(111) and MoC(111) surface used to calculate the free energy diagrams on Figure 5.

	NH	NH_2	NH_3	NNH	NNH_2	NHNH	$NHNH_2$	NH_2NH_2
MoC(111)	-6.02	3.89	-1.50	-3.19	-4.83	-5.05	-3.80	-2.02
$MoC_{0.5}$(111)	-6.01	-3.71	-1.39	-3.71	-5.24	-5.18	-3.65	-1.98

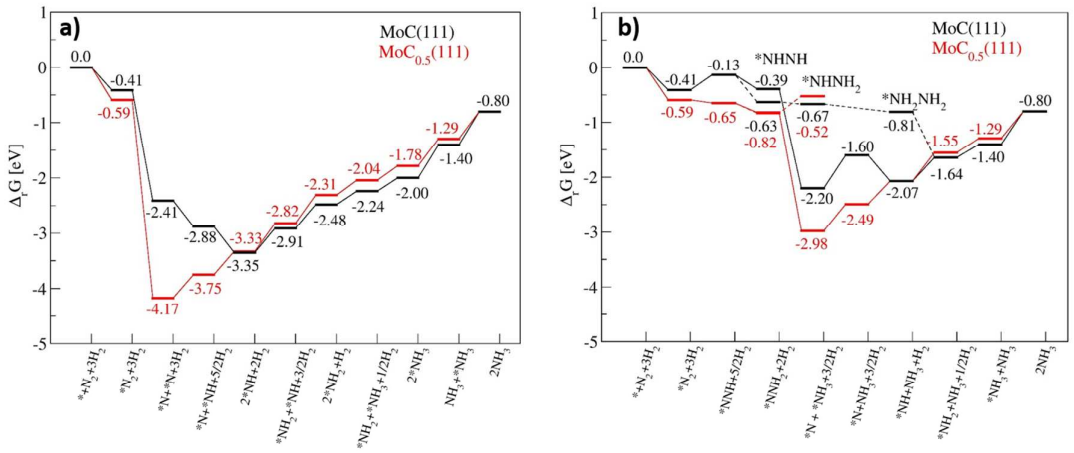

Figure 5. DFT calculated free energy diagram for nitrogen electroreduction on the (111) surface of MoC and $MoC_{0.5}$ compositions a) dissociative Heyrovsky mechanism and b) associative Heyrovsky mechanism.

In the case of the Mo:C=2:1 ratio, the potential-determining step in the dissociative mechanism of nitrogen electroreduction is the same as in the case of MoC composition, requiring the energy of +0.51 eV. Thus, slightly more negative potential of -0.51 V *vs* standard hydrogen electrode will be needed to drive the formation of ammonia on $MoC_{0.5}$ composition. However, the desorption of ammonia, $*NH_3 \rightarrow NH_3(g)$ is slightly less uphill on $MoC_{0.5}$(111) surface than on the MoC(111) surface, indicating that the introduction of carbon vacancies slightly increases overpotential for nitrogen reduction, but might have a beneficial effect on the release of the product.

3.3.2. Associative mechanism

As can be seen from Figure 5b, adsorption of nitrogen is exergonic on the MoC(111) surface with the free energy change of -0.41 eV followed by the endergonic step in which the adsorbed nitrogen is hydrogenated to form adsorbed *NNH with the change in the free energy of +0.28 eV. The nitrogen reduction on MoC(111) can then proceed by two different paths, to form $*NNH_2$ after which the N-N nitrogen bond breaking occurs to produce *N and $NH_3(g)$. In the alternative path, addition of hydrogen atom to *NNH leads to the formation of adsorbed *NHNH, which gets further hydrogenated to from adsorbed $*NH_2NH_2$. Hydrogenation of $*NH_2NH_2$ leads to the N-N bond breaking step and the formation of $*NH_2$ and ammonia. Further two steps, hydrogenation of $*NH_2$ to form $*NH_3$ and desorption of NH_3 are both endothermic with the change in the free energy of +0.24 eV and +0.60 eV. This indicates that the potential determining step for the associative mechanism on the cubic MoC phase is the first hydrogenation of adsorbed nitrogen of +0.28 eV, which requires less energy than the most endergonic step in the dissociative mechanism.

In the case of associative mechanism of nitrogen electroreduction on the $MoC_{0.5}$(111) the first two steps, which lead to the adsorption of nitrogen molecule and the hydrogenation of adsorbed N_2 to from *NNH, are exergonic. The free energy diagram also shows that the N-N bond breaking step occurs during the hydrogenation of adsorbed $*NNH_2$ due to the large stability of adsorbed nitrogen atom and adsorbed ammonia and small stability of adsorbed $*NHNH_2$ species. The following steps that include the hydrogenation of the adsorbed nitrogen are endergonic. As such,

the potential limiting step for the associative mechanism on $MoC_{0.5}$(111) is the same as for the dissociative mechanism. The onset potential for both mechanisms is determined by the $*NH+H^{+}+e^{-} \rightarrow *NH_2$ step with the energy change of +0.51 eV. The potential of at least -0.5 V will be required to drive the complete electroreduction of nitrogen to ammonia on the $MoC_{0.5}$(111) surface.

Based on these results we can conclude that the MoC(111) surface is active for electroreduction of ammonia. Potential needed to drive the reduction is determined to be at least -0.3 V in the case of the MoC composition and at least -0.5 V in the case of the $MoC_{0.5}$ composition. This indicates smaller overpotential for the reduction of nitrogen to ammonia on the MoC composition. Furthermore, it was determined that on the cubic MoC electroreduction of nitrogen to ammonia follows energetically more favourable associative mechanism, which is also identified as the mechanism of enzyme-catalysed ammonia synthesis.[2, 53] However, it needs to be emphasized that desorption of ammonia is an uphill process and can still limit the overall reaction by poisoning the catalytic surface with the product at low temperatures.

As partial conversion of a carbide to a nitride could be expected under the standard ammonia electro-synthesis conditions, it is also interesting to compare these results with our previous studies on molybdenum nitride, Mo_2N, which is isostructural to herein considered $MoC_{0.5}$.[11] Our results show that $MoC_{0.5}$ and MoC share some similar features to those of Mo_2N, namely both materials can bind nitrogen in bridging positions that activates the N-N bond. $MoC_{0.5}$ and Mo_2N both have high affinity of N-adatoms, which prevents the accumulation on H-adatoms at low cell potentials. However, the (111) surfaces of both MoC and $MoC_{0.5}$ composition are found to have lower overpotentials for nitrogen reduction (slightly less negative onset potentials) than Mo_2N. Namely, the cell potentials needed to drive the reduction of nitrogen to ammonia was found to be -0.7 V on Mo_2N(111) surface while it was found to be -0.5 V and -0.3 V on the $MoC_{0.5}$(111) and MoC(111) surface. MoC and $MoC_{0.5}$ are also characterized by slightly lower interaction with ammonia (0.6 and 0.5 eV) than Mo_2N (0.9 eV), which means that the molybdenum carbide will be more resilient to poisoning of the catalytic surface with ammonia at lower temperatures that the nitride. Another difference between the nitrogen electroreduction on molybdenum carbide and molybdenum nitride has to be emphasized. Namely, the electroreduction of nitrogen on cubic MoC is expected to prefer associative Heyrovsky path, while our previous study had shown that nitrogen electroreduction on molybdenum nitride will be able to follow both associative and dissociative mechanism.

3.3.3. Desorption of ammonia

As we have found that desorption of ammonia is critical for the successful formation of ammonia from nitrogen on both MoC and $MoC_{0.5}$ compositions, we further studied the influence of the surface structure on desorption of NH_3 (Figure 6). Based on DFT calculations desorption of ammonia is predicted to be endergonic on all MoC surfaces, however it is predicted to be exergonic on $MoC_{0.5}$(001) and $MoC_{0.5}$(100) surfaces and endergonic on (111), (101), (111)* and (311) surfaces of $MoC_{0.5}$. Change in the free Gibbs energy for ammonia desorption is calculated as +0.08 eV, +0.61 eV, +0.60 eV, +0.45 eV and +0.28 eV on the MoC[100], MoC[110], MoC(111), MoC(111)*, and MoC(311) surface, while it is calculated as -0.20 eV, -0.05 eV, +0.27 eV, +0.49 eV, +0.40 eV, and +0.37 eV on $MoC_{0.5}$(001), $MoC_{0.5}$(100)/(010), $MoC_{0.5}$(101), $MoC_{0.5}$(111), $MoC_{0.5}$(111)*, and $MoC_{0.5}$(311) surfaces, respectively.

Therefore, based on these results we can conclude that the high index surfaces, defects and carbon vacancies are beneficial for the nitrogen electroreduction to ammonia as they promote the release of product from the catalytic surface. The (111) surface of MoC is predicted to have high activity for nitrogen electroreduction, but the existence of under-coordinated surface Mo atoms becomes critical as the surface defects and carbon vacancies promote ammonia desorption.

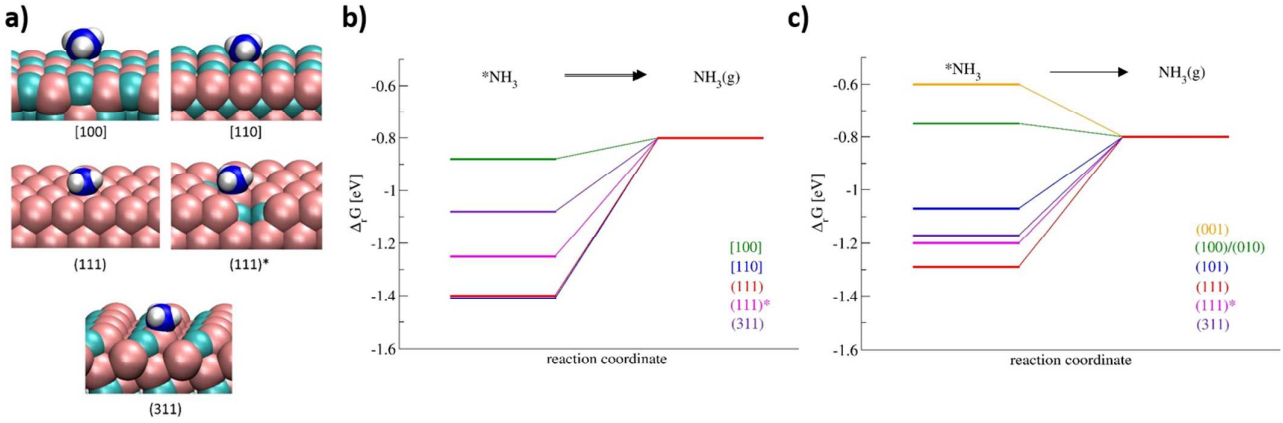

Figure 6. a) DFT calculated geometries of ammonia adsorbed on MoC. DFT calculated free energy change for desorption of ammonia on different surfaces of cubic molybdenum carbide with b) MoC and c) $MoC_{0.5}$ composition.

Journal Name

ARTICLE

Conclusions

Density functional theory was used to study the energetics of adsorption of molecular nitrogen, atomic nitrogen, and ammonia on various crystallographic surfaces of cubic MoC. The MoC(111), MoC(111)*, and MoC(311) surface are predicted to have high activity for nitrogen adsorption and dissociation. However, the MoC(111) is the only surface at which hydrogen evolution might be suppressed at low cell potentials due to the larger stability region of N-adatoms relative to that of H-adatoms. Based on the free energy diagrams for nitrogen electroreduction to ammonia on MoC(111), it was also found that low negative potential of at least -0.3 V relative to standard hydrogen electrode is needed to drive the reduction of nitrogen to ammonia. The electroreduction of nitrogen on MoC(111) surface is expected to follow associative Heyrovsky path in which N-N bond breaks after partial hydrogenation of the adsorbed nitrogen molecule. Desorption of ammonia is an endergonic process on all MoC surfaces and will become a thermodynamically limiting step at low temperatures, which can be partially mitigated by the introduction of steps or Mo and C vacancies. Namely, our results show that higher index surfaces and defects decrease the interaction with the adsorbed ammonia and promote its release from the catalytic surface.

Free energy diagrams and kinetic volcano plots for hydrogen evolution reaction point that the [110] surface of cubic MoC has high activity for hydrogen evolution reaction. The comparison between the Gibbs free energies for formation of H-adatoms and N-adatoms on the cubic MoC with 1:1 and 2:1 ratio of Mo and C atoms shows that the stability region of H-adatoms is smaller on $MoC_{0.5}$ than on MoC. Namely, increasing metal to carbon ratio increases the affinity of the catalytic surface for N-adatoms due to the presence of carbon vacancies in the bulk and prevents the accumulation of H-adatoms.

The complexity of the presented results points to the challenges in the design of catalysts with high activity and selectivity for nitrogen electroreduction to ammonia at ambient conditions. Namely, as evidenced by our computational results and by the previous experimental observations, the same material will often have catalytic sites/surfaces with high activity for nitrogen reduction and hydrogen evolution, which decreases the efficiency of electrochemical synthesis of ammonia. The high selectivity would, therefore, require the design of materials that will maximize the exposure of specific crystallographic surfaces. In addition, under standard ammonia electro-synthesis conditions, the carbide surface structure can be converted to a nitride, leading to the changes in the activity and the pathways of the nitrogen electroreduction process. This would require additional changes in the reaction conditions to ensure the stability of the certain phase/chemical composition of the carbide.

Conflicts of interest

There are no conflicts to declare.

Acknowledgements

This work was supported by the Advanced Research Projects Agency-Energy (ARPA-E), U.S. Department of Energy, under Award Number DE-AR 1261-4005. VASP license was provided by Theoretical division, LANL, which is supported by the Office of Science of the U.S. Department of Energy under Contract No. DE-AC52-06NA25396. Computational work was performed using the computational resources of EMSL, a national scientific user facility sponsored by the Department of Energy's Office of Biological and Environmental Research and located at Pacific Northwest National Laboratory, NERSC, supported by the Office of Science of the U.S. Department of Energy under Contract No. DE-AC02-05CH11231, and CNMS, sponsored at Oak Ridge National Laboratory by the Scientific User Facilities Division, Office of Basic Energy Sciences, U.S. Department of Energy. This paper has been designated LA-UR-18-21724.

References

1 S. Giddey, S. P. S. Badwal and A. Kulkarni, *Int. J. Hydrogen Energ.*, 2013, **38**, 14576-14594.
2 C. J. M. van der Ham, M. T. M. Koper and D. G. H. Hetterscheid, *Chem. Soc. Rev.*, 2014, **43**, 5183-5191.
3 G. Marnellos and M. Stoukides, *Science*, 1998, **282**, 98.
4 V. Kyriakou, I. Garagounis, E. Vasileiou, A. Vourros and M. Stoukides, *Catal. Today*, 2017, **286**, 2-13.
5 J. K. Nørskov, T. Bligaard, B. Hvolbaek, F. Abild-Pedersen, I. Chorkendorff and C. H. Christensen, *Chem. Soc. Rev.*, 2008, **37**, 2163-2171.
6 C. J. H. Jacobsen, S. Dahl, B. S. Clausen, S. Bahn, A. Logadottir and J. K. Nørskov, *J. Am. Chem. Soc*, 2001, **123**, 8404-8405.
7 E. Skúlason, T. Bligaard, S. Gudmundsdottir, F. Studt, J. Rossmeisl, F. Abild-Pedersen, T. Vegge, H. Jonsson and J. K. Nørskov, *Phys. Chem. Chem. Phys.*, 2012, **14**, 1235-1245.
8 J. G. Howalt, T. Bligaard, J. Rossmeisl and T. Vegge, *Phys. Chem. Chem. Phys.*, 2013, **15**, 7785-7795.
9 J. G. Howalt and T. Vegge, *Phys. Chem. Chem. Phys.*, 2013, **15**, 20957-20965.
10 J. G. Howalt and T. Vegge, *Beilstein J. Nanotechnol.*, 2014, **5**, 111-120.

11 I. Matanovic, F. H. Garzon and N. J. Henson, *Phys. Chem. Chem. Phys.*, 2014, **16**, 3014-3026.
12 J. H. Montoya, C. Tsai, A. Vojvodic and J. K. Nørskov, *ChemSusChem*, 2015, **8**, 2180-2186.
13 Y. Abghoui, A. L. Garden, J. G. Howalt, T. Vegge and E. Skúlason, *ACS Catalysis*, 2016, **6**, 635-646.
14 Y. Abghoui and E. Skúlason, *Catal. Today*, 2017, **286**, 78-84.
15 M.-T. Nguyen, N. Seriani and R. Gebauer, *Phys. Chem. Chem. Phys.*, 2015, **17**, 14317-14322.
16 I. A. Amar, R. Lan, C. T. G. Petit and S. Tao, *Electrocatal.*, 2015, **6**, 286-294.
17 N. Ji, T. Zhang, M. Zheng, A. Wang, H. Wang, X. Wang and J. G. Chen, *Angew. Chem. Int. Ed.*, 2008, **47**, 8510-8513.
18 A. L. Stottlemyer, T. G. Kelly, Q. Meng and J. G. Chen, *Surf. Sci. Rep*, 2012, **67**, 201-232.
19 P. Liu and J. A. Rodriguez, *J. Phys. Chem. B*, 2006, **110**, 19418-19425.
20 F. Viñes, J. A. Rodriguez, P. Liu and F. Illas, *J. Catal.*, 2008, **260**, 103-112.
21 W. Zheng, T. P. Cotter, P. Kaghazchi, T. Jacob, B. Frank, K. Schlichte, W. Zhang, D. S. Su, F. Schüth and R. Schlögl, *J. Am. Chem. Soc.*, 2013, **135**, 3458-3464.
22 S. T. Oyama, *Catal. Today*, 1992, **15**, 179-200.
23 R. Kojima and K.-i. Aika, *Appl. Catal., A*, 2001, **219**, 141-147.
24 J. R. d. S. Politi, F. Vines, J. A. Rodriguez and F. Illas, *Phys. Chem. Chem. Phys.*, 2013, **15**, 12617-12625.
25 J. Kouvetdkis and L. J. Brewer, *J. Phase Equilibria.*, 1992, **13**, 601-604.
26 T. Xiao, A. P. E. York, K. S. Coleman, J. B. Claridge, J. Sloan, J. Charnock and M. L. H. Green, *J. Mater. Chem.*, 2001, **11**, 3094-3098.
27 J. S. Lee, L. Volpe, F. H. Ribeiro and M. Boudart, *J. Catal.*, 1988, **112**, 44-53.
28 B. G. Demczyk, J. G. Choi and L. T. Thompson, *Appl. Surf. Sci.*, 1994, **78**, 63-69.
29 J.-G. Choi, R. L. Curl and L. T. Thompson, *J. Catal.*, 1994, **146**, 218-227.
30 G. L. W. Hart and B. M. Klein, *Phys. Rev. B*, 2000, **61**, 3151-3154.
31 S. Posada-Pérez, P. J. Ramírez, J. Evans, F. Viñes, P. Liu, F. Illas and J. A. Rodriguez, *J. Am. Chem. Soc.*, 2016, **138**, 8269-8278.
32 S. Posada-Perez, R. A. Gutierrez, Z. Zuo, P. J. Ramirez, F. Vines, P. Liu, F. Illas and J. A. Rodriguez, *Catal. Sci. Technol.*, 2017, **7**, 5332-5342.
33 A. Mª. Gómez-Marín and E. Ticianelli, *Electrochim. Acta*, 2016, **220**, 363-372.
34 C. He and J. Tao, *RSC Adv.*, 2016, **6**, 9240-9246.
35 J. S. Kang, J. Kim, M. J. Lee, Y. J. Son, D. Y. Chung, S. Park, J. Jeong, J. M. Yoo, H. Shin, H. Choe, H. S. Park and Y.-E. Sung, *Adv. Sci.*, 2018, **5**, 1700601-n/a.
36 J. P. Perdew, K. Burke and M. Ernzerhof, *Phys. Rev. Lett.*, 1996, **77**, 3865-3868.
37 J. P. Perdew, K. Burke and M. Ernzerhof, *Phys. Rev. Lett.*, 1997, **78**, 1396-1396.
38 P. E. Blöchl, *Phys. Rev. Lett.*, 1994, **B 50**, 17953-17979.
39 G. Kresse and J. Joubert, *Phys. Rev. B*, 1999, **59**, 1758-1775.
40 G. Kresse and J. Hafner, *Phys. Rev. B*, 1993, **47**, 558-561.
41 G. Kresse and J. Hafner, *Phys. Rev. B*, 1994, 14251-14269.
42 G. Kresse and J. Furthmüller, *Comput. Mat. Sci.*, 1996, **6**, 15-50.
43 G. Kresse and J. Furthmüller, *Phys. Rev. B*, 1996, **54**, 11169-11186.
44 H. J. Monkhorst and J. D. Pack, *Phys. Rev. B: Condens. Matter Mater Phys.*, 1976, **13**, 5188-5192.
45 M. Methfessel and A. T. Paxton, *Physical Review B*, 1989, **40**, 3616-3621.
46 P. W. Atkins, *Physical Chemistry*, Oxford University Press, Oxford, 1998.
47 J. K. Nørskov, J. Rossmeisl, A. Logadottir, L. Lindqvist, J. R. Kitchin, T. Bligaard and H. Jónsson, *J. Phys. Chem. B*, 2004, **108**, 17886-17892.
48 J. Rossmeisl, J. K. Nørskov, C. D. Taylor, M. J. Janik and M. Neurock, *J. Phys. Chem. B*, 2006, **110**, 21833-21839.
49 J. K. Nørskov, T. Bligaard, A. Logadottir, J. R. Kitchin, J. G. Chen, S. Pandelov and U. Stimming, *J. Electrochem. Soc.*, 2005, **152**, J23-26.
50 J. Greeley, T. F. Jaramillo, J. Bonde, I. Chorkendorff and J. K. Nørskov, *Nat. Mater.*, 2006, **5**, 909.
51 Y. Zheng, Y. Jiao, Y. Zhu, L. H. Li, Y. Han, Y. Chen, A. Du, M. Jaroniec and S. Z. Qiao, *Nat. Commun.*, 2014, **5**, 3783.
52 J. Heyrovsky, *Recl. Trav. Chim. Pays-Bas*, 1927, **46**, 582.
53 T. H. Rod, A. Logadottir and J. K. Nørskov, *J. Chem. Phys.*, 2000, **112**, 5343-5347.